Equilibrium return times of small fluctuating clusters and vacancies

Francesco Boccardo, Younes Benamara, and Olivier Pierre-Louis*
Institut Lumière Matière, UMR5306 Université Lyon 1 - CNRS, 69622 Villeurbanne, France

(Received 30 May 2022; accepted 3 August 2022; published 22 August 2022)

The expected return time of a fluctuating two-dimensional cluster or vacancy to a given configuration is studied in thermodynamic equilibrium. We define a family of bond-breaking models that preserve the number of particles. This family includes edge diffusion and surface diffusion inside vacancies in the limit of fast particle diffusion and slow attachment-detachment kinetics. Within the frame of these bond-breaking models, the expected return time is found to depend on the energies of the configurations and on the energies of the excited states formed by removing a single particle from the cluster. High- and low-temperature regimes are studied. We clarify the conditions under which the return time is a nonmonotonous function of temperature: a minimum is found when the energy obtained by the average over the excited states of the configuration weighted by their attachment probabilities is lower than the energy averaged over all states. In addition, we show that the optimal temperature at which the return time is minimum is shifted to a higher temperature as compared to the temperature at which the equilibrium probability is maximum. This shift is influenced by the average curvature of the cluster edge, and is therefore larger for vacancies.

DOI: 10.1103/PhysRevE.106.024120

I. INTRODUCTION

Two-dimensional monolayer clusters of atoms or particles have been studied extensively in the past decades. Since the 1990s, advances in visualization techniques such as scanning tunnelling microscopy for atomic monolayer clusters [1,2] and confocal microscopy for colloid monolayer clusters [3] have enabled their accurate observation up to the the atom or particle scale. These observations led to the characterization of equilibrium shape fluctuations [1,2,4,5] that are caused by the random diffusion of their constituent atoms or particles, both for monolayer clusters [4–6], and monolayer vacancies [6–13].

The static equilibrium properties of these fluctuations obey well-known equilibrium statistical mechanics [14], and their experimental observation can be used to determine energetic properties of the cluster edge in atomic clusters [15,16] and colloid clusters [17,18]. In contrast, the dynamical properties of the fluctuations are sensitive to the kinetics of the relevant mass transport mechanisms. Theoretical investigations of the dynamics of fluctuations have been developed using Langevin models [19–21] or kinetic Monte Carlo simulations of lattice models for clusters [6,22–28] and vacancies [29–31]. These modeling studies mostly aimed at predicting the diffusion of the whole cluster or the time correlation functions of edge fluctuations. In the following, we focus on a different kinetic property of small fluctuating clusters: their time of return to a given configuration. This focus is motivated by our recent attempt to describe first passage times from one arbitrary configuration to another [32]. These first passage times were evaluated numerically using iterative evaluation techniques in Ref. [32]. The expected return time from a configuration to itself exhibits similar properties as the first passage times [32] and is an easier starting point for numerical and analytical approaches.

In the present paper, we therefore report on the evaluation of the equilibrium's expected return time to a given configuration. We work with an extended class of models that allows us to discuss not only the case of clusters with edge diffusion (ED) [32] but also the case of particle diffusion inside vacancies with slow attachment-detachment kinetics. The expressions derived here lead to simpler and faster estimates of the expected return times as compared to the numerical evaluation based on iterative evaluation [32]. They also lead to an easier and generalized analysis of the high-temperature expansion discussed in Ref. [32]. Furthermore, they allow us to perform low-temperature expansions to determine activation energies. Finally, the analysis of the expression of the return time provides a simple interpretation for the appearance of an optimal temperature at which the return time is minimum for configurations with low energy.

We start in Sec. II by showing that the expected return time depends on the expected residence time in the configuration and on the equilibrium distribution via the well-known Kac lemma [33,34]. We distinguish two different definitions of the return time that differ only by the fact of taking into account the time spent on the configuration itself.

In section Sec. III, we define a class of broken-bond dynamical models with single particle moves that preserve the cluster area. We focus on two specific models belonging to this class, namely, clusters with ED and vacancies with detachment, diffusion inside the vacancy, and reattachment (DDA) of atoms or particles in the limit of slow interface kinetics.

A discussion of the equilibrium distribution is then reported in Sec. IV. High- and low-temperature expansions are presented. We notice that configurations with low energy

*olivier.pierre-louis@univ-lyon1.fr

exhibit an optimal temperature for which their equilibrium probability is maximum. This optimal equilibrium temperature corresponds to the temperature at which the energy of the configuration is equal to the thermodynamic average of the energy. The maximum exists only when the energy of the configuration is lower than the average of the energy over all configurations.

The return time to a given configuration is discussed in Sec. V. Within the broken-bond models, the expression of the residence times can be written as a function of the energies of the excited states that are obtained by removing a single atom from the cluster. High- and low-temperature expansions of the return times are discussed. We clarify the physical origin of the optimal temperature at which large enough low-energy clusters were found to exhibit a minimum return time in Ref. [32]. We show that a minimum is present when the average energy of the excited states of the configuration weighted by attachment probabilities is lower than the average energy over all configurations. This return time optimal temperature is found to be shifted to higher temperatures as compared to the optimal temperature of the equilibrium distribution. In addition, we show that the change of sign of the edge curvature between clusters and vacancies leads to an increased shift toward high temperatures for vacancies. Finally, the two different definitions of the return time are seen to be similar in most cases, except for very small clusters and for square islands of arbitrary size at low temperatures.

II. RELATION BETWEEN MEAN RETURN TIME, RESIDENCE TIME, AND EQUILIBRIUM DISTRIBUTION

Let us start with some general and standard relations to define our cluster as a dynamical stochastic system at equilibrium.

In the following, the configuration (or shape) of the cluster is called the state of the cluster, and denoted by s. The physical behavior of the system is described by the rates $\gamma(s, s')$ for the transition from a state s of the cluster to a state s'. We assume Markovian dynamics, and the system obeys the master equation

$$\partial_t P(s,t) = \sum_{s' \in \mathcal{B}_s} [\gamma(s', s)P(s', t) - \gamma(s, s')P(s, t)], \tag{1}$$

where $P(s, t)$ is the probability that the system is in state s at time t, and $\mathcal{B}_s$ is the set of all states different from s that can be reached in one transition from s.

In equilibrium, the probability $P_{\rm eq}(s)$ to be in state s is independent of time and obeys

$$P_{\rm eq}(s) = \frac{e^{-H_s/T}}{\sum_{s' \in \mathcal{S}} e^{-H_{s'}/T}}, \tag{2}$$

where H_s is the Hamiltonian, i.e., the energy of the state s, T is the temperature in units where the Boltzmann constant is equal to 1, and $\mathcal{S}$ is the set of all states, which is assumed to be finite.

We assume that the cluster dynamics is constrained by detailed balance,

$$P_{\rm eq}(s)\gamma(s, s') = P_{\rm eq}(s')\gamma(s', s), \tag{3}$$

which directly enforce stationarity in Eq. (1). In addition, we have from the combination of Eqs. (2) and (3):

$$\gamma(s, s')e^{-H_s/T} = \gamma(s', s)e^{-H_{s'}/T}. \tag{4}$$

Let us now consider a situation where we observe the system during a long time, paying particular attention to a given state s. Due to ergodicity, state s will be reached. After reaching state s, the cluster will visit other states different from s. Later, the system will come back again to s, and so on. Let us denote $t^{\rm obs}$ the total observation time and $t^{\rm tot}(s)$ the total time spent on state s during this observation time. It is clear that since we are in equilibrium, the equilibrium probability $P_{\rm eq}(s)$ is the fraction of time spent in state s, and is therefore

$$P_{\rm eq}(s) = \lim_{t^{\rm obs}\to\infty} \frac{t^{\rm tot}(s)}{t^{\rm obs}}. \tag{5}$$

Then, let us define the loop number n_ℓ as the number of times the system passes on the state s. The expected residence time $t(s)$ in state s obeys [35]

$$t(s) = \lim_{t^{\rm obs}\to\infty} \frac{t^{\rm tot}(s)}{n_\ell}. \tag{6}$$

Remark that the expected residence time of a state s is the average of the time before a transition to a different state $s' \neq s$. As a consequence, the transitions that directly take the system from s to itself are discarded and are not considered as loops.

Moreover, we define the expected loop time $\tau^\ell(s)$ as the average period of the return to the state s, so

$$\tau^\ell(s) = \lim_{t^{\rm obs}\to\infty} \frac{t^{\rm obs}}{n_\ell}. \tag{7}$$

Combining Eqs. (5)–(7), we obtain a form of the well-known Kac lemma [33,34],

$$\tau^\ell(s) = \frac{t(s)}{P_{\rm eq}(s)}, \tag{8}$$

which relates the loop time $\tau^\ell(s)$ to the stationary distribution $P_{\rm eq}(s)$. In the literature, $\tau^\ell(s)$ is often called the expected return time to state s. However, following the definition of Ref. [32], we define the expected return time $\tau^{\rm r}(s)$ as the expected time spent outside state s before returning to it. We therefore have

$$\tau^{\rm r}(s) = \tau^\ell(s) - t(s) = t(s)\left(\frac{1}{P_{\rm eq}(s)} - 1\right). \tag{9}$$

In Eqs. (8) and (9), the equilibrium distribution is given by Eq. (2), and the residence time can be written directly as a function of the rates:

$$t(s) = \frac{1}{\sum_{s' \in \mathcal{B}_s} \gamma(s, s')}. \tag{10}$$

Note that our definitions imply that physical events that do not change state s of the system are not listed in the transitions in Eq. (10).

As a summary, the knowledge of the energies H_s and of the rates $\gamma(s, s')$ allows one to determine the expected return time. To analyze the consequences of this simple result for thermal

fluctuations of few-particles clusters, we need to define more precisely the kinetics of the model, which is determined by the rates $\gamma(s, s')$.

III. BROKEN-BOND MODELS

A. Model definitions

We consider a two-dimensional cluster on a square lattice with lattice parameter a and nearest-neighbor bond energy J. A cluster is defined as a part of the lattice composed of N sites that are connected to each other through nearest neighbors. Two cluster configurations are considered to be different if they cannot be obtained one from the other via translations. This makes our definition of cluster states identical to that of free polyominoes or free lattice animals [36]. Vacancies are defined in a similar way as a set of empty connected sites in a full monolayer.

The dynamics is assumed to result from moves that involve only one particle at a time. The number of different moves that can take the system from state s to state s' is denoted as $k_{ss'}$. These moves from s to s' are indexed by $k = 1, .., k_{ss'}$. We assume that each move has a reverse move. Hence, the reverse moves can also be indexed by the same index k, and the total number of moves between states s and s' is the same as the number of reverse moves:

$$k_{ss'} = k_{s's}. \tag{11}$$

Following the usual models for activation of particle or atom diffusion [37–39], the rate of the transition from state s to state s' due to the kth one-particle move is assumed to take an Arrhenius form

$$\gamma_k(s, s') = \nu\, b_{ss';k}\, e^{-n_{ss';k} J/T}, \tag{12}$$

where ν is an attempt frequency, $n_{ss';k}$ is the number of in-plane nearest neighbors of the moving particle in state s before hopping, and $b_{ss';k}$ is a model-dependent attachment probability. The total transition rate from s to s' therefore reads

$$\gamma(s, s') = \sum_{k=1}^{k_{ss'}} \gamma_k(s, s'). \tag{13}$$

In addition, for consistency, the rates vanish for moves that are not authorized, i.e., $\gamma(s, s') = 0$ when $k_{ss'} = 0$.

The rates Eq. (12) define a family of models which correspond to different ways of setting the possible moves and the associated parameters $b_{ss';k}$. Each physical model for the re-attachment of the particles after detachment provides a specific expression of $b_{ss';k}$. Here we consider four basic constraints on the reattachment rules. First, particles always reattach after detachment, so the number of particles in the cluster is not changed. Second, particles reattach instantaneously. This means that we assume that the time needed for the reattachment process is negligible as compared to the time of detachment. Third, we assume that all detachment-reattachment moves have a reverse move. This condition is necessary to enforce detailed balance at equilibrium Eq. (3). Finally, the detachment-reattachment moves do not break the cluster into disconnected clusters.

Within this family of detachment reattachment processes, we wish to focus on two types of dynamics described schematically in Fig. 1. The first model is ED dynamics of particle clusters. Various models have been developed to describe ED in atomic monolayer clusters (see, e.g., Refs. [23,40] and references therein). Here, we choose to use a simple model following the rules of Refs. [32,41]. In this case, the particles reattach to nearest-neighbor or next-nearest neighbor sites along the edge of the cluster, i.e., to sites that have at least one nearest-neighbor bond with another particle of the cluster. Moreover, we choose

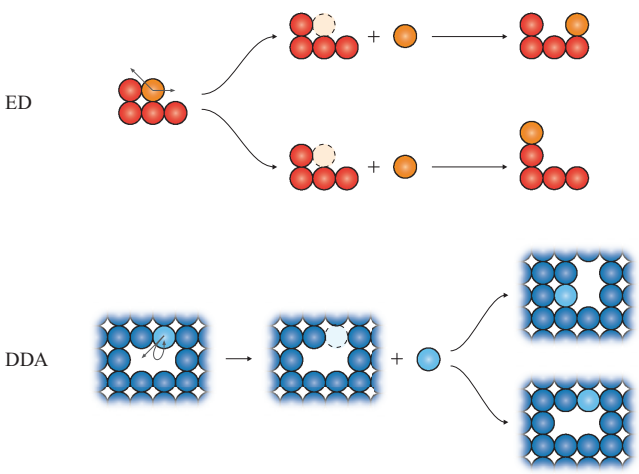

FIG. 1. Schematics of particle moves within the two broken-bond models discussed here. In red, cluster with edge diffusion (ED). In blue, vacancy with particle detachment-diffusion-reattachment (DDA). In each case, the arrows in the leftmost schematic indicate the possible moves of the atom in lighter color. Intermediate states after the detachment of one particle are called excited states. The states after one move are shown in the rightmost panels. Note that the final state in the lower right panel is identical to the initial state.

$$b_{ss';k} = 1. \tag{14}$$

With this choice, we aim at describing the different possible moves of a particle as independent processes.

The second model accounts for DDA of particles inside vacancies. In this case, the moves are composed of a chain of three processes: first detachment, then diffusion, and then reattachment. Reattachment can occur on any site at the edge inside the cluster with the same probability. This model corresponds to a regime where reattachment is slower than diffusion, so particles have ample time to diffuse inside the cluster before reattaching. In such a situation, the probability of presence of the atom inside the cluster has time to relax to a spatially homogeneous probability and, as a consequence, we can choose an attachment probability that is independent of the position of the attachment site [42]. We therefore have

$$b_{ss';k} = \frac{1}{\ell^{\dagger}_{ss';k}}, \tag{15}$$

where $\ell^{\dagger}_{ss';k}$ is the number of sites for the particle to reattach along the edge of the cluster. As an example, for the move of the dimer vacancy on Fig. 1, there are two possible attachment sites (described by the red arrows) so that $\ell^{\dagger}_{ss';k} = 2$.

For consistency, we also forbid configurations where an isolated, nonmobile particle is inside the vacancies. This

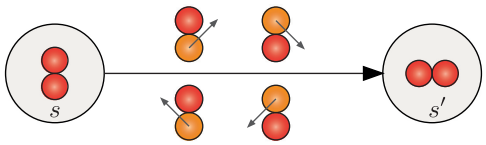

FIG. 2. Different particle moves can lead to the same transition. Here, we consider a dimer cluster $N = 2$ with edge diffusion. The transition from one state to the other can be achieved in four different ways. Hence $k_{ss'} = 4$.

condition adds novel constraints on the moves that are imposed in addition to the nonbreaking constraints. It also leads to a reduced number of states for vacancies as compared to clusters.

The total number of moves $k_{ss'}$ from state s to state s' depends on the model and can be larger than 1. For example, there are four possible moves for the transition of a dimer cluster with ED shown in Fig. 2. The dependence of $k_{ss'}$ on N is summarized in Fig. 3. In the cluster ED model, $k_{ss'} = 4$ for the two transitions of the dimers with $N = 2$ particles, and $k_{ss'} = 1$ for $N \geqslant 3$, as already noted in Ref. [32]. In the vacancy DDA model, $k_{ss'}$ is decreasing as N increases, but there are moves with $k_{ss'} = 2$ for any N. However, as seen in Fig. 3, these moves are rare in the sense that the average $\langle\langle k_{ss'}\rangle_{s'\in\mathcal{B}_s}\rangle_{s\in\mathcal{S}}$ over all possible moves tends quickly to 1 as the number N of particles in the cluster increases. For any set of states $\mathcal{Z}$, we have defined the average of a state-dependent function f_s as

$$\langle f_s\rangle_{s\in\mathcal{Z}} = \frac{1}{|\mathcal{Z}|}\sum_{s\in\mathcal{Z}} f_s, \tag{16}$$

with $|\mathcal{Z}|$ the cardinal of $\mathcal{Z}$. Moreover, we recall that $\mathcal{S}$ is the set of all possible states for a fixed size N, and $\mathcal{B}_s$ is the set of all states different from s that can be reached in one transition from s.

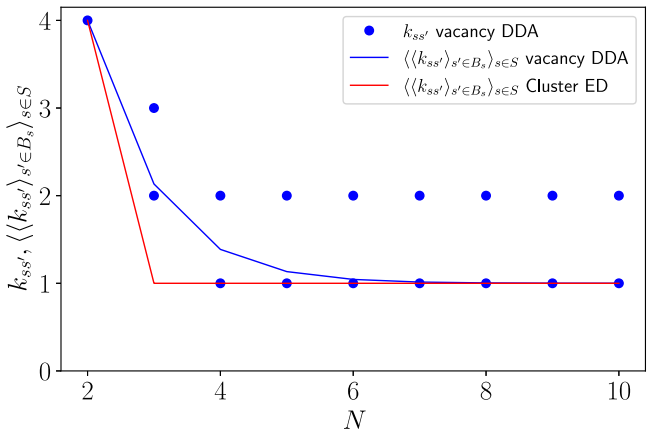

FIG. 3. Number of different moves $k_{ss'}$ to go from a state s to another state s' as a function of cluster size N. The symbols show all possible values of $k_{ss'}$ within the two models, cluster ED and vacancy DDA. The solid lines correspond to the average value $\langle\langle k_{ss'}\rangle_{s'\in\mathcal{B}_s}\rangle_{s\in\mathcal{S}}$ of $k_{ss'}$ over all possible moves.

B. Hamiltonian and excited states

The broken bond model is directly related to the Ising or lattice-gas lattice models. As discussed, e.g., in Refs. [14,43], the energy of a cluster in state s is simply related to the length L_s of its edge:

$$H_s = \frac{J}{2}\frac{L_s}{a}. \tag{17}$$

A simple intuitive interpretation of this result is that the breaking of a bond costs an energy J and increases the length of the edge by $2a$. The energy cost for the formation of an elementary segment of the edge of length a is therefore $J/2$, and we recover Eq. (17).

As seen from Fig. 1, an atomic move which allows for the transition from state s to state s' can be decomposed into two stages. In the first stage, we create an excited state by breaking all the bonds that the atom has in its initial condition. This excited state can be interpreted as the situation where the particle is brought to the saddle point of the diffusion energy landscape. In the second stage, we reattach the atom.

Let us denote excited states with a † symbol. We define the Hamiltonian of the excited state $H^\dagger_{ss';k}$ as the Hamiltonian of the state obtained by removing the detaching particle during the kth particle move that leads to the transition from s to s'. We then have

$$H^\dagger_{ss';k} = \frac{J}{2}\frac{L^\dagger_{ss';k}}{a} + 2J, \tag{18}$$

where $L^\dagger_{ss';k}$ is the length of the edge of the cluster obtained by removing the moving atom. In the examples shown in Fig. 1, $L^\dagger_{ss';k} = 10$ for cluster ED and $L^\dagger_{ss';k} = 8$ for vacancy DDA. The additional constant $2J$ in Eq. (18) accounts for the energy of the detached particle. Indeed, since a detached particle has four broken bonds and each broken bond costs an energy $J/2$, its total broken-bond energy is $4J/2 = 2J$. Note that the excited state for the kth transition $s \to s'$ is the same as the excited state for the kth transition $s' \to s$. We therefore have

$$L^\dagger_{ss';k} = L^\dagger_{s's;k}, \quad H^\dagger_{ss';k} = H^\dagger_{s's;k}. \tag{19}$$

The change of cluster edge length when removing a single atom is related to the number bonds $n_{ss';k}$ that are broken via [14]

$$L^\dagger_{ss';k} - L_s = 2a(n_{ss';k} - 2). \tag{20}$$

As a consequence, the activation energy of Eq. (12) reads

$$n_{ss';k}J = 2J + \frac{J}{2a}(L^\dagger_{ss';k} - L_s) = H^\dagger_{ss';k} - H_s. \tag{21}$$

This latter equation indicates that the product $n_{ss';k}J$ can be decomposed into two parts: the excited state energy $H^\dagger_{ss';k}$ which is identical for the move and its reverse, and the energy of the initial state H_s. In other words, the energy barrier for detachment is the difference between the energy of the excited state, which play the role of an effective saddle point for the energy, and the energy of the initial state. Combining

Eqs. (12), (13), (21), the rates may now be written as

$$\gamma(s,s') = \nu\, e^{H_s/T} \sum_{k=1}^{k_{ss'}} b_{ss';k}\, e^{-H^{\dagger}_{ss';k}/T}. \tag{22}$$

Moreover, the cluster ED and vacancy DDA models both obey the symmetry relation

$$b_{ss';k} = b_{s's;k}. \tag{23}$$

This relation is trivially valid for cluster ED as seen from Eq. (14). In the case of vacancy DDA, the number of sites $\ell^{\dagger}_{ss';k}$ to which detached particles can be reattached is a property of the kth excited state between states s and s'. As a consequence, we have $\ell^{\dagger}_{ss';k} = \ell^{\dagger}_{s's;k}$ in Eq. (15) and the symmetry property Eq. (23) follows.

Since Eq. (22) is the product of $e^{H_s/T}$ with a factor that is invariant under the exchange of indices $s \leftrightarrow s'$, the rates $\gamma(s,s')$ are seen to obey detailed balance Eq. (4). Hence, the broken-bond models exhibit a well-defined equilibrium state characterized by the energies Eq. (17).

In the following, we will use units where $J = 1$, $a = 1$ and $\nu = 1$.

IV. EQUILIBRIUM DISTRIBUTION

A. Energy levels

The energy of a cluster can only explore a finite number of energy levels indexed by $i = 0, 1, \ldots, i_{\max}$, with energy $H_{(i)}$ corresponding to a given edge length $L_{(i)} = 2H_{(i)}$. The energy levels obey

$$L_{(i)} = L_{(0)} + 2i, \quad H_{(i)} = \frac{L_{(i)}}{2} = H_{(0)} + i, \tag{24}$$

where the ground-state energy $H_{(0)} = L_{(0)}/2$ depends on the size N of the cluster.

The number of states that correspond to the energy level i is denoted as $G_{(i)}$. We also define the total number of states:

$$S_N = \sum_{i=0}^{i_{\max}} G_{(i)}. \tag{25}$$

For $N = 2$ and $N = 3$, there is only one energy level and $i_{\max} = 0$. We have $G_{(0)} = S_2 = 2$ for $N = 2$, and $G_{(0)} = S_3 = 6$ for $N = 3$. The values of $G_{(i)}$ and S_N obtained by explicit enumeration for $4 \leqslant N \leqslant 12$ are reported in Fig. 4. These numbers are different for clusters and vacancies because of the prohibition of isolated particles inside vacancies which appear for $N \geqslant 7$. However, the difference is small as compared to $G_{(i)}$ itself, as seen from Figs. 4(b) and 4(c). When $N \gg 1$, we expect S_N to be well approximated by the asymptotic form [36]:

$$S_N \approx c\lambda^N/N. \tag{26}$$

The parameters of this asymptotic form are well-known for free polyominoes, which correspond exactly to our clusters: $\lambda \approx 4.0626$ and $c \approx 0.3169$ [44]. Vacancies have a slightly lower S_N, the asymptotic form of which is not known. However, we expect that clusters and vacancies should have the same value of λ [45].

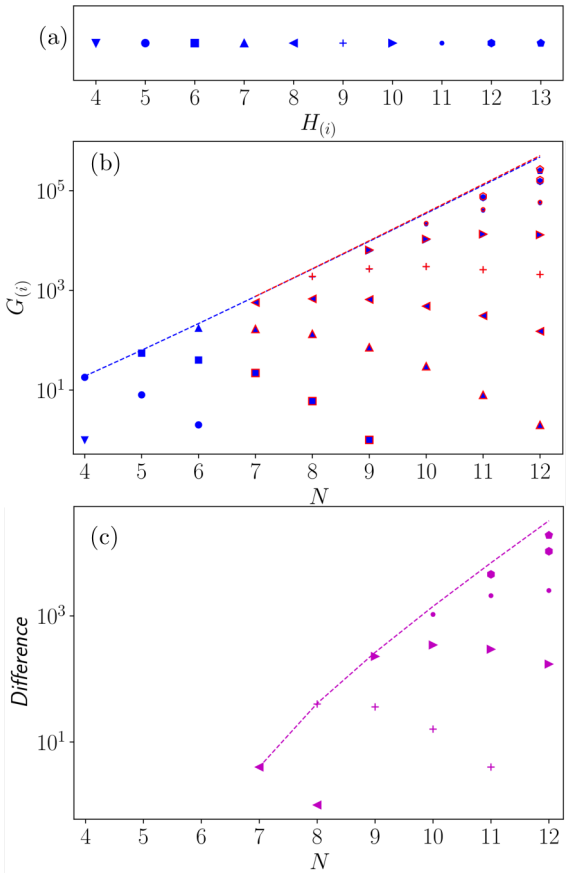

FIG. 4. Degeneracy $G_{(i)}$ of different energy levels i. Each symbol corresponds to a different value of energy, reported in the scale in (a). (b) Degeneracies $G_{(i)}$. Red empty symbols and blue full symbols, respectively, correspond to clusters and vacancies. The total number of states S_N is also reported as a dashed line. (c) Difference between the degeneracies $G_{(i)}$ of clusters and vacancies.

In Fig. 5, the equilibrium probability distribution $P_{\rm eq}(s)$ given by Eq. (2) is plotted as a function of the inverse temperature for various energy levels i. The case reported in Fig. 5 corresponds to a vacancy octamer $N = 8$, with four energy levels $i = 0, 1, 2, 3$. The case of a cluster with $N = 8$ is not plotted but is very similar.

As expected, the equilibrium distribution decreases as i increases. However, the temperature dependence of $P_{\rm eq}$ is less trivial. In Fig. 5, $P_{\rm eq}$ is seen to increase monotonously as the temperature is decreased for the ground state $i = 0$, and decreases monotonously for large i. Interestingly, $P_{\rm eq}$ exhibit a maximum for intermediate values of i. This nonmonotonic behavior can be understood intuitively. Indeed, at very low temperatures the cluster stays in the ground states $i = 0$. As the temperature increases, higher energy levels are populated and the corresponding values of $P_{\rm eq}$ increase. In contrast, in the limit of very high temperatures, all states are populated equally and $P_{\rm eq} \to P_\infty$ as $1/T \to 0$, with

$$P_\infty = \frac{1}{S_N}. \tag{27}$$

When the temperature is decreased from this high temperature limit, the states with a lower energy become more probable

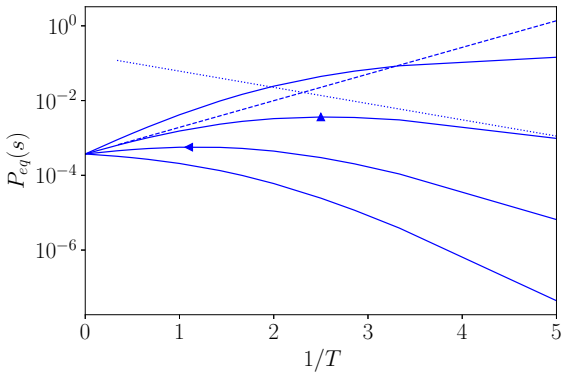

FIG. 5. Equilibrium probability distribution for vacancies with $N = 8$. The solid lines correspond to $P_{\rm eq}$. There are four energy levels with $i = 0, 1, 2, 3$ from top to bottom, corresponding to energies $H_{(i)} = H_{(0)} + i$ where $H_{(0)} = 6$ is the ground-state energy. The dashed and dotted lines, respectively, report the high- and low-temperature expansions. Symbols indicate the maximum of $P_{\rm eq}$.

while those with a higher energy become less probable. Thus, since their probability increases when starting both from the very low temperature limit and from the very high temperature limit, low-energy states that are not the ground state must exhibit a maximum at some finite temperature. We call this temperature the optimal equilibrium temperature $T_{\rm m}^{\rm eq}$ because this corresponds to the temperature where the probability of observing a given state is highest. The position of the maximum is marked by a symbol in Fig. 5.

B. High- and low-temperature expansions

A high temperature expansion of Eq. (2) to first order in $1/T$ leads to

$$P_{\rm eq}(s) \underset{T\to\infty}{\longrightarrow} P_\infty\left[1 + \frac{M_{\rm eq}(s)}{T}\right],$$
$$M_{\rm eq}(s) = \langle H_{s'}\rangle_{s'\in\mathcal{S}} - H_s, \tag{28}$$

where the infinite temperature equilibrium distribution $P_\infty = 1/S_N$ is independent of the state s.

In the opposite limit at low temperatures, we have

$$P_{\rm eq}(s) \underset{T\to 0}{\longrightarrow} \frac{1}{G_{(0)}} e^{(H_{(0)}-H_s)/T}, \tag{29}$$

where $H_{(0)}$ is the ground-state energy of the cluster of size N and $G_{(0)}$ is the number of different states that have the ground state energy $H_{(0)}$.

C. Equilibrium optimal temperature

As seen from Fig. 5 and discussed above, the ground state exhibits a monotonously increasing $P_{\rm eq}$ when decreasing the temperature. Thus, combining Eqs. (28) and (29), a simple criterion for the presence of a maximum at finite temperature is that the energy of the state is lower than the average energy over all states:

$$H_{(0)} < H_s < \langle H'_s\rangle_{s\in\mathcal{S}}. \tag{30}$$

This inequality indicates that clusters with a low energy exhibit a finite temperature $T_m^{\rm eq}(s)$ that maximizes the equilibrium probability $P_{\rm eq}(s)$. Note that this temperature depends only on the energies of the system, not on the kinetics.

In general, the condition of a maximum of $P_{\rm eq}(s)$ reads $\partial_T P_{\rm eq}(s) = 0$, leading to an implicit equation for the optimal equilibrium temperature:

$$H_s = \overline{H_{\rm eq}}|_{T=T_m^{\rm eq}(s)}, \tag{31}$$

where we have defined the thermodynamic average of the energy:

$$\overline{H_{\rm eq}} = \sum_{s'\in\mathcal{S}} H_{s'} P_{\rm eq}(s'). \tag{32}$$

A first estimation of the temperature $T_m^{\rm eq}(s)$ at which $P_{\rm eq}(s)$ is maximum can be obtained from a comparison of the high- and low-temperature expansions Eqs. (28) and (29). Assuming that $T_m^{\rm eq}(s)$ corresponds to the temperature $T_{\rm a}^{\rm eq}(s)$, where both expressions are equal, and reformulating the high-temperature expansion as $P_{\rm eq}(s) \approx S_N^{-1} \exp[M_{\rm eq}(s)/T]$, we find

$$T_{\rm a}^{\rm eq} = \frac{\langle H_{s'}\rangle_{s'\in\mathcal{S}} - H_{(0)}}{\ln\left[\frac{S_N}{G_{(0)}}\right]}. \tag{33}$$

Such a temperature corresponds to the crossing of the high- and low-temperature approximations shown in Fig. 5. Note that this approximate expression does not depend on state s, and depends only on the cluster size N. As seen from Fig. 6, the inverse temperature $1/T_{\rm a}^{\rm eq}$ provides a fair account of the average of $1/T_m^{\rm eq}(s)$ over the energy levels for a given cluster size N. However, $T_{\rm a}^{\rm eq}$ is not an accurate estimate as it does not account for the strong dispersion of the optimal temperatures depending on the energy-level i.

A high-temperature expansion of Eq. (31) to first order in the inverse temperature $1/T$ leads to another approximate expression of the optimal equilibrium temperature of a state s belonging to the energy level i:

$$T_{\rm HT}^{\rm eq} = \frac{\langle H_{s'}^2\rangle_{s'\in\mathcal{S}} - \langle H_{s'}\rangle_{s'\in\mathcal{S}}^2}{\langle H_{s'}\rangle_{s'\in\mathcal{S}} - H_{(0)} - i}. \tag{34}$$

As expected, this estimate is seen to account well for the optimal temperature when $1/T_m^{\rm eq}$ is small in Fig. 6(a). However, this expression underestimates lower optimal temperatures, which corresponds to larger values of $1/T_m^{\rm eq}$.

In the opposite limit of low temperatures, we first notice that the ground state can be considered as a state with an optimal temperature at zero temperature. This statement is indeed in agreement with Eq. (31) and is intuitively associated to the presence of a horizontal tangent of the curve $P_{\rm eq}(s)$ in Fig. 5. For states in higher energy levels $i \geqslant 1$, an expansion of Eq. (31) to first order in the low-temperature small parameter $\exp[-1/T]$ suggests

$$T_{\rm LT}^{\rm eq} = \frac{1}{\ln\frac{G_{(1)}}{iG_{(0)}}}. \tag{35}$$

However, note that the smallness $\exp[-1/T]$ requires that $iG_{(0)}/G_{(1)} \ll 1$. In general, low-temperature expansions are delicate because they require a precise knowledge of the variation of $G_{(i)}$ with i an N, which is still an open problem [36]. The comparison reported in Fig. 6(b) shows a fair a agreement

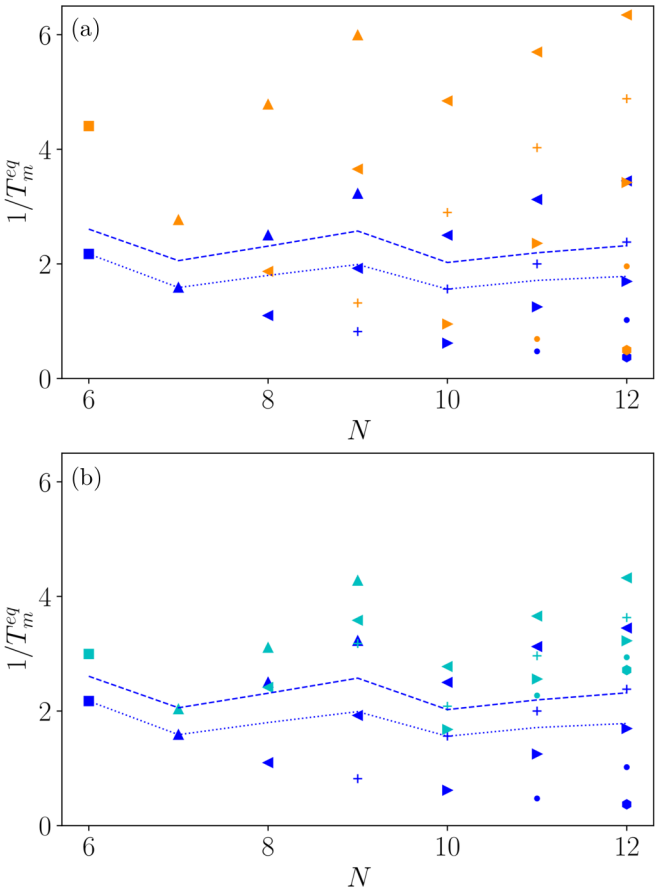

FIG. 6. Equilibrium optimal temperature $T_m^{\rm eq}$ as a function of N for different energy levels i. We show the case of vacancies (clusters are very similar). The optimal temperature $T_m^{\rm eq}$ is in blue (dark) symbols. The symbols correspond to the energies in the scale at the top of Fig. 4. The dashed lines represent $1/T_a^{\rm eq}$ from Eq. (33), and the dotted line is the average of the inverse optimal temperatures over energy levels. In (a), the optimal temperatures are compared to the high-temperature approximation Eq. (34) in orange (light) symbols. In (b), the optimal temperatures are compared to the low-temperature approximation Eq. (35) in cyan (light) symbols.

between Eq. (35) and the lowest optimal temperatures corresponding to $i = 1$. However, $T_{\rm LT}^{\rm eq}$ is not accurate for higher energy levels.

V. RETURN TIMES

A. Expression of $\tau^{\rm r}(s)$

Combining Eqs. (2), (9), (10), and (22), we obtain an expression of the expected return time,

$$\tau^{\rm r}(s) = \frac{\sum_{s'\in\mathcal{S}\backslash s} e^{-H_{s'}/T}}{\sum_{s'\in\mathcal{B}_s}\sum_{k=1}^{k_{ss'}} b_{ss';k}\, e^{-H^{\dagger}_{ss';k}/T}}, \tag{36}$$

where $\mathcal{S}\backslash s$ is the set of all states but the state s. We recall that our definition of the residence time discards the moves that take the system from a state s to itself. An example of a move that does not change state s is shown at the bottom of Fig. 1.

In the limit where $T \to \infty$, all exponential terms in Eq. (36) are equal to 1. Then Eq. (36) leads to a generalization

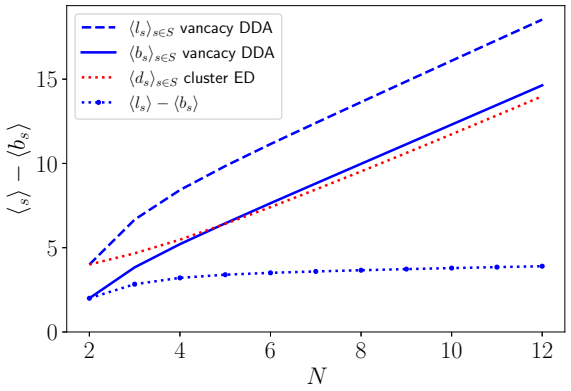

FIG. 7. Average b degree as a function of N. For cluster ED, we have $\langle d_s\rangle_{s\in\mathcal{S}} = \langle b_s\rangle_{s\in\mathcal{S}}$. For vacancy DDA, we show both $\langle b_s\rangle_{s\in\mathcal{S}}$ and the average number of particles $\langle \ell_s\rangle_{s\in\mathcal{S}}$ that can be detached in state s as a function of N.

of the well-known formula [46] for return times $\tau^{\rm r}_\infty(s)$ on graphs with equal rates,

$$\tau^{\rm r}_\infty(s) = \frac{S_N - 1}{b_s}, \tag{37}$$

where we have defined the b degree:

$$b_s = \sum_{s'\in\mathcal{B}_s}\sum_{k=1}^{k_{ss'}} b_{ss';k}. \tag{38}$$

The b degree b_s differs from the standard graph theoretic definition of degree d_s of state s. The degree d_s is defined on a graph where the vertices are the states and the edges are the moves [32]. Then the degree d_s is the number of edges incident to a given vertex s, which corresponds to the total number of single-particle moves from state s [32] [47]:

$$d_s = k_{ss} + \sum_{s'\in\mathcal{B}_s} k_{ss'}. \tag{39}$$

Note that $k_{ss'} \geqslant 1$ for $s' \in \mathcal{B}_s$ by definition. However, we can have $k_{ss} = 0$ when $s' = s$. There are two differences between Eqs. (39) and (38). The first difference is that b_s is a weighted sum with weight $b_{ss';k}$ for each move. The second difference is that the sum over $\mathcal{B}_s$ discards moves that take the system back to the starting state s in Eq. (39).

In the case of cluster ED, we have $b_{ss';k} = 1$ and there is no move which takes the system directly back to the initial state s (i.e., $k_{ss} = 0$). Hence, b_s is equal to the degree d_s. Then Eq. (37) reduces to the well-known formula [32,46] $\tau^{\rm r}_\infty(s) = (S_N - 1)/d_s$. The average $\langle d_s\rangle_{s\in\mathcal{S}}$ for clusters is shown in Fig. 7 as a function of N.

In the case of vacancy DDA, the values of b_s and d_s are different. Some intuition on the physical meaning of b_s can be gained by combining Eqs. (15) and (39), leading to [48]

$$b_s = \ell_s - \sum_{q=1}^{\ell_s} \frac{1}{\ell^{\dagger}_{s;q}}, \tag{40}$$

where ℓ_s is the number of particles that can be detached in state s, and $q = 1, .., \ell_s$ is an index for these particles. We have also defined the number $\ell^{\dagger}_{s;q}$ of possible attachment sites in the

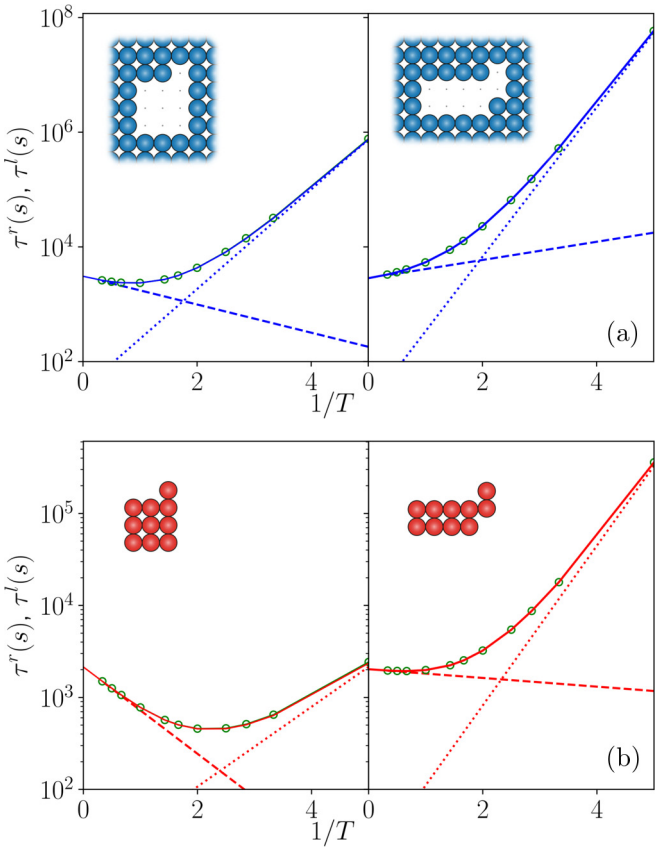

FIG. 8. Expected return time $\tau^{\mathrm{r}}(s)$ for two clusters with $N = 10$ as a function of the inverse temperature $1/T$. (a) Vacancy DDA. (b) Cluster ED. The dashed and dotted lines correspond, respectively, to high- and low-temperature expansions. The green empty symbols correspond to the loop time $\tau^{\ell}(s)$. In the left panels, $H_s = 7$ and $i = 0$. I the right panels, $H_s = 8$ and $i = 1$.

excited state obtained by removing the qth particle. We expect $\ell_s^{\dagger}$ and $\ell_{s;q}^{\dagger}$ to be of the same order of magnitude because they both increase with edge length. However, many attachment sites are forbidden in very ramified vacancies because they would lead to breaking, so, on average, $\ell_{s;q}^{\dagger}$ is smaller than $\ell_s^{\dagger}$. We therefore expect that the second term on the right-hand side of Eq. (40) to be larger than 1. As seen in Fig. 7, the difference $\ell_s - b_s$ grows slowly as N increases, and reaches maximum values around 4 in the range $N \leqslant 12$ than we have investigated.

Using Eq. (37), the return time to target is rewritten as

$$\tau^{\mathrm{r}}(s) = \tau^{\mathrm{r}}_{\infty}(s) \frac{\langle e^{-H_{s'}/T} \rangle_{s' \in \mathcal{S}\setminus s}}{\langle\langle e^{-H^{\dagger}_{ss';k}/T} \rangle\rangle_{k,s' \in \mathcal{B}_s}}, \tag{41}$$

where we have defined a new averaging notation for any quantity $f_{ss';k}$,

$$\langle\langle f_{ss';k} \rangle\rangle_{k,s' \in \mathcal{B}_s} = \frac{1}{b_s} \sum_{s' \in \mathcal{B}_s} \sum_{k=1}^{k_{ss'}} b_{ss';k}\, f_{ss';k}, \tag{42}$$

that corresponds to a weighted average over all possible moves from state s with weights $b_{ss';k}$.

In Fig. 8, the return time evaluated from the equivalent expressions Eqs. (36) and (41) is shown for different cluster shapes and for the two models. The expressions Eqs. (36) and (41) are in quantitative agreement with numerical estimates based on the iterative evaluation method reported in Ref. [32] for ED. Here, we have implemented this iterative method both for cluster ED and vacancy DDA. Perfect agreement is found between iterative evaluation and the expressions based on Kac's formula Eqs. (36) and (41). Technical details on the implementation of iterative evaluation and a comparison between the two methods are reported in Appendix A.

In Ref. [32], we have noticed that $\tau^{\mathrm{r}}(s)$ can exhibit a minimum as a function of temperature T for particle cluster ED. In Fig. 8(a), we see that this minimum can also be present for vacancy DDA.

B. High-temperature expansion

A high-temperature expansion of Eq. (41) to linear order in $1/T$ leads to

$$\begin{aligned} \tau^{\mathrm{r}}(s) &\xrightarrow[T\to\infty]{} \tau^{\mathrm{r}}_{\infty}(s)\left(1 + \frac{M^{\mathrm{r}}(s)}{T}\right), \\ M^{\mathrm{r}}(s) &= \langle\langle H^{\dagger}_{ss';k} \rangle\rangle_{k,s' \in \mathcal{B}_s} - \langle H_{s'} \rangle_{s' \in \mathcal{S}\setminus s} \\ &= \langle\langle H^{\dagger}_{ss';k} \rangle\rangle_{k,s' \in \mathcal{B}_s} - \langle H_{s'} \rangle_{s' \in \mathcal{S}} \\ &\quad + \frac{1}{S_N - 1}(H_s - \langle H_{s'} \rangle_{s' \in \mathcal{S}}). \end{aligned} \tag{43}$$

In the case of cluster ED, this expression is in agreement with the result of Ref. [32]. However, this result was not written as a function of energies in Ref. [32]. The derivation of Eqs. (43) using the method presented in Ref. [32] is discussed in detailed in Appendix B.

One of the main statements of Ref. [32] was that the expected return time for large and compact states exhibits a minimum at a finite temperature. Such a minimum is associated to the condition of a negative slope at high temperature ($1/T \to 0$) in the plots of Fig. 8, i.e., $M^{\mathrm{r}}(s) < 0$. As N increases, S_N grows exponentially and the terms in the last line of the expression of $M^{\mathrm{r}}(s)$ in Eq. (43) should be negligible. In addition, the contribution of the state s to the average $\langle H_{s'} \rangle_{s' \in \mathcal{S}\setminus s}$ should be negligible, so that $\langle H_{s'} \rangle_{s' \in \mathcal{S}\setminus s} \approx \langle H_{s'} \rangle_{s' \in \mathcal{S}}$. Hence, the criterion $M^{\mathrm{r}}(s) < 0$ for the presence of a minimum can be written approximately as

$$\langle\langle H^{\dagger}_{ss';k} \rangle\rangle_{k,s' \in \mathcal{B}_s} < \langle H_{s'} \rangle_{s' \in \mathcal{S}}. \tag{44}$$

This condition is one of our main results.

In Figs. 9(a) and 9(b), we have reported the average energy $\langle H_{s'} \rangle_{s' \in \mathcal{S}}$ as a function of N. Since higher energy levels have higher degeneracy $G_{(i)}$ (as seen from Fig. 4), the value of $\langle H_{s'} \rangle_{s' \in \mathcal{S}}$ is close to the maximum possible value of the energy $H_{\max} = H_{(i_{\max})} = N + 1$.

In addition, the values of $\langle\langle H^{\dagger}_{ss';k} \rangle\rangle_{k,s' \in \mathcal{B}_s}$ for all possible transitions to states s' are shown in Fig. 9(a) when starting from a ground state s with $i = 0$, and in Fig. 9(b) when starting from the first excited state s with $i = 1$. As a first remark, due to the average curvature of the interface, atoms that detach from the edge of vacancies have, on average, more bonds to break. Thus, the excited state energies of vacancies are higher. This is seen for $i = 0$ and $i = 1$ in Fig. 9.

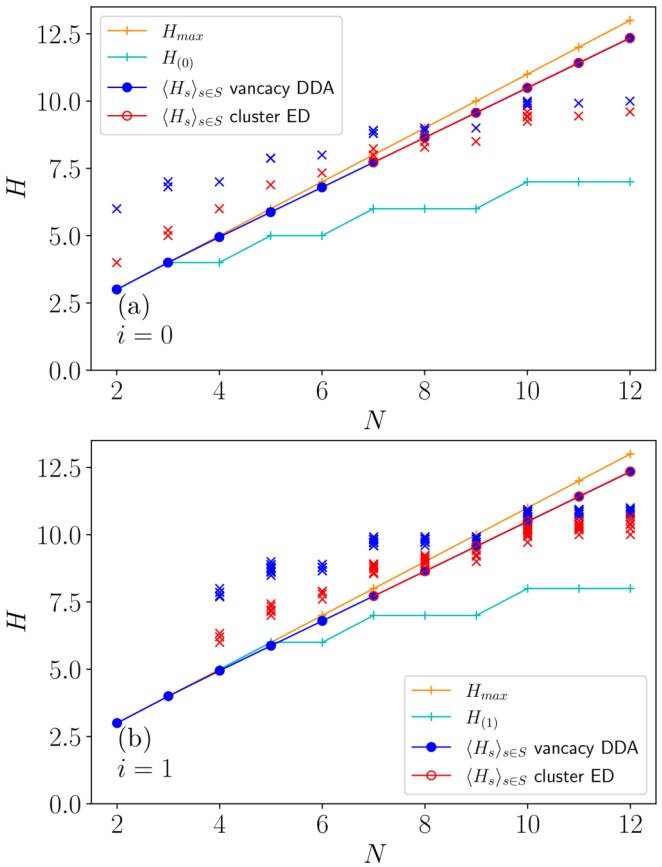

FIG. 9. Comparison of different energies as a function of N (a) for ground states with $i = 0$ and (b) for states in the first energy level with $i = 1$. Cyan pluses: Energy $H_{(i)}$ of the states. Blue and red circles: average energy $\langle H_{s'}\rangle_{s'\in\mathcal{S}}$ for vacancies and clusters, respectively (these data points are almost identical). Orange pluses: Maximum energy $H_{\max} = N + 1$. Blue and red crosses: All possible values of $\langle\langle H^{\dagger}_{ss';k}\rangle\rangle_{k,s'\in\mathcal{B}_s}$.

A close inspection of Figs. 9(a) and 9(b) shows that for a given i, a given N, and a given model (cluster ED or vacancy DDA), the values of $\langle\langle H^{\dagger}_{ss';k}\rangle\rangle_{k,s'\in\mathcal{B}_s}$ are either all above $\langle H_{s'}\rangle_{s'\in\mathcal{S}}$, or all below $\langle H_{s'}\rangle_{s'\in\mathcal{S}}$. Moreover, the value of N above which $\langle\langle H^{\dagger}_{ss';k}\rangle\rangle_{k,s'\in\mathcal{B}_s}$ is below $\langle H_{s'}\rangle_{s'\in\mathcal{S}}$ depends on i and on the model. For cluster ED, a minimum is predicted when $N \geqslant 8$ with $i = 0$, and when $N \geqslant 9$ with $i = 1$. For vacancy DDA, a minimum is predicted when $N \geqslant 9$ with $i = 0$, and when $N \geqslant 11$ with $i = 1$.

These conditions for $i = 0$ and $i = 1$ are in agreement with the observation of a minimum in the return time of the ground states. For example, let us consider Fig. 8, where $N = 10$, $i = 0$ in the left panels, and $i = 1$ in the right panels. A minimum is observed for clusters with $i = 0$ and $i = 1$ and for vacancies only when $i = 0$, in agreement with the above statements.

C. Low-temperature expansion

The expression Eq. (36) also allows one to obtain an asymptotic low-temperature expression for the expected return time. For states s that are not a ground state, i.e., $H_s > H_{(0)}$, we have

$$\tau^{\mathrm{r}}(s) \underset{T\to 0}{\longrightarrow} \frac{G_{(0)}}{G^{\dagger}_{s(0)}} e^{(H^{\dagger}_{s(0)} - H_{(0)})/T}, \tag{45}$$

where we recall that $G_{(0)}$ is the number of different configurations that correspond to the ground state with energy $H_{(0)}$. Moreover, we have defined $H^{\dagger}_{s(0)}$ as the lowest energy over all excited states of a state s, and

$$G^{\dagger}_{s(0)} = \sum_{s'\in\mathcal{B}_s} \sum_{k\,|\,H^{\dagger}_{ss';k} = H^{\dagger}_{s(0)}} b_{ss';k}, \tag{46}$$

where the sum on k is performed only on the moves that take the cluster to the excited state with the lowest energy, i.e., $H^{\dagger}_{ss';k} = H^{\dagger}_{s(0)}$.

When the state s is a ground state, i.e., $H_s = H_{(0)}$ the contribution that dominates the denominator of Eq. (36) at low temperature depends on the fact that the ground state is unique or not. If the ground state is not unique, i.e., if $G_{(0)} \geqslant 2$, then

$$\tau^{\mathrm{r}}(s) \underset{T\to 0}{\longrightarrow} \frac{G_{(0)} - 1}{G^{\dagger}_{s(0)}} e^{(H^{\dagger}_{s(0)} - H_{(0)})/T}. \tag{47}$$

However, if the ground state is unique, i.e., $G_{(0)} = 1$, the contribution that dominates the denominator of Eq. (36) at low temperatures is the energy level $i = 1$ just above the ground state. Using Eq. (24), we then find

$$\tau^{\mathrm{r}}(s) \underset{T\to 0}{\longrightarrow} \frac{G_{(1)}}{G^{\dagger}_{s(0)}} e^{(H^{\dagger}_{s(0)} - H_{(0)} - 1)/T}. \tag{48}$$

Since this latter case of a unique ground state only occurs for square clusters, Eq. (48), only applies in the specific case of square clusters.

The low-temperature expansions Eqs. (45) and (47) are shown in Fig. 8 for a state in the energy level $i = 1$ (right panel) and for a nonunique ground state (left panels).

D. Return time optimal temperature

The optimal return time temperature is the temperature at which $\tau^{\mathrm{r}}(s)$ is minimum. This temperature is a kinetic quantity that depends on the dynamical properties of the system. When $\tau^{\mathrm{r}}(s)$ exhibit an optimal temperature $T^{\mathrm{r}}_m(s)$ where it is minimum, then $\partial_T \tau^{\mathrm{r}}(s) = 0$. Applying this condition on Eq. (41) leads to

$$\frac{\left\langle H_{s'} e^{-H_{s'}/T^{\mathrm{r}}_m(s)}\right\rangle_{s'\in\mathcal{S}\setminus s}}{\left\langle e^{-H_{s'}/T^{\mathrm{r}}_m(s)}\right\rangle_{s'\in\mathcal{S}\setminus s}} = \left.\frac{\overline{H_{\mathrm{eq}}} - H_s P_{\mathrm{eq}}(s)}{1 - P_{\mathrm{eq}}(s)}\right|_{T = T^{\ell}_m(s)}$$
$$= \frac{\left\langle\left\langle H^{\dagger}_{ss';k}\, e^{-H^{\dagger}_{ss';k}/T^{\mathrm{r}}_m(s)}\right\rangle\right\rangle_{k,s'\in\mathcal{B}_s}}{\left\langle\left\langle e^{-H^{\dagger}_{ss';k}/T^{\mathrm{r}}_m(s)}\right\rangle\right\rangle_{k,s'\in\mathcal{B}_s}}, \tag{49}$$

where the expression in the right hand side of the first line is a direct rewriting of the left-hand side. In Fig. 10, the optimal return time inverse temperature $1/T^{\mathrm{r}}_m(s)$ is plotted for various states s with different size N. These temperatures are obtained by means of a direct numerical estimate of the temperature at which $\tau^{\mathrm{r}}(s)$ is minimum.

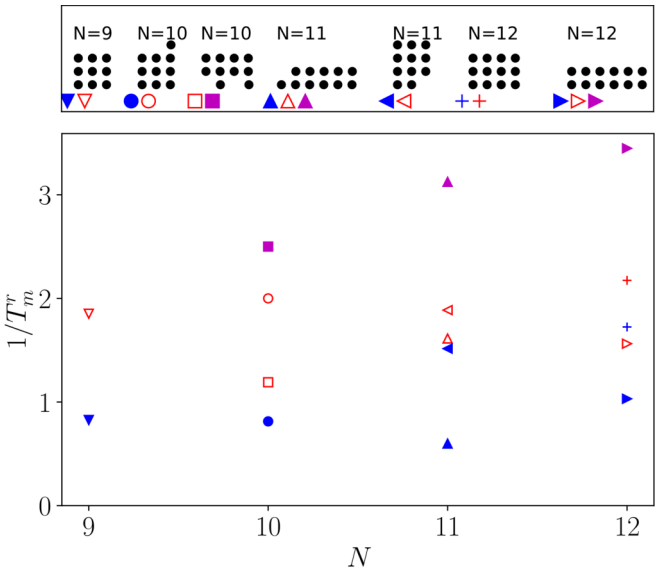

FIG. 10. Inverse optimal return time temperature $1/T_m^r(s)$ for the states listed in the top panel. Blue (dark) symbols: Vacancy DDA. Red (empty) symbols: cluster ED. Violet (lighter) symbols: Inverse of the equilibrium optimal temperature $1/T_m^{\rm eq}$ when it is finite ($T_m^{\rm eq}$ exhibits very similar values for vacancy DDA and cluster ED). For ground states ($i = 0$), corresponding to the first, second, fifth, and sixth clusters on the top panel, $1/T_m^{\rm eq} \to \infty$ is not shown.

We observe that the values of $T_m^{\rm r}(s)$ in Fig. 10 are actually higher than the corresponding equilibrium optimal temperatures $T_m^{\rm eq}(s)$. This can be explained from an inspection of Eq. (9) which states that $\tau^{\rm r}(s)$ is the product of $t(s)$ with $1/P_{\rm eq}(s) - 1$. Indeed, $T_m^{\rm eq}(s)$ corresponds to a minimum of the factor $1/P_{\rm eq}(s) - 1$. Since $P_{\rm eq}(s)$ is very similar for particle clusters and vacancy clusters as discussed in Sec. IV, this factor can be considered to be identical in these two cases for our qualitative discussion. In addition, all rates $\gamma(s, s')$ decrease with temperature due to their Arrhenius form, so $t(s)$ which is the inverse of a sum of rates from Eq. (10), increases with decreasing temperature. In general, the product of a monotonic function with a function with a minimum leads to a function with a shifted minimum. Here, due to the monotonic decrease of the residence time $t(s)$ with temperature, the minimum $T_m^{\rm r}(s)$ of the product $t(s)(1/P_{\rm eq}(s) - 1)$ is shifted to a higher temperature as compared to the minimum $T_m^{\rm eq}(s)$ of $(1/P_{\rm eq}(s) - 1)$. As a consequence, $T_m^{\rm r}(s)$ is always higher than $T_m^{\rm eq}(s)$:

$$T_m^{\rm r}(s) > T_m^{\rm eq}(s). \tag{50}$$

This inequality is confirmed by Fig. 10, where the inverse equilibrium temperature $1/T_m^{\rm eq}(s)$ is either infinite for ground states (as discussed in Sec. IV C, a ground state can be considered as a state with $T_m^{\rm eq}(s) = 0$) or finite and plotted in purple for non-ground states. We see in Fig. 10 that the associated inverses of the return time optimal temperatures $1/T_m^{\rm r}(s)$ are always smaller than $1/T_m^{\rm eq}(s)$.

Because of this shift toward higher temperatures, low-temperature approximations for $T_m^{\rm r}(s)$ are not accurate. Nevertheless, a high-temperature expansion can be performed from Eq. (49). Its detailed expression and a comparison with the true optimal temperature is reported in Appendix C.

Finally, another general feature of $T_m^{\rm r}(s)$ can be observed. Indeed, as already noted in Sec. V B, the excited state energies of vacancies are higher due to the curvature of the edge. As a consequence of their higher excited state energies, the decrease of $t(s)$ with temperature [see Eqs. (10) and (22)] is actually faster for vacancies. Hence, the shift of the optimal temperature toward higher temperatures is stronger for vacancies, leading to a higher return time optimal temperature $T_m^{\rm r}(s)$. This effect is systematically observed in Fig. 10.

E. Comparison between $\tau^{\rm r}(s)$ and $\tau^{\ell}(s)$

The expected loop time exhibits an expression similar to that of the return time,

$$\tau^{\ell}(s) = \tau_{\infty}^{\ell}(s) \frac{\langle e^{-H_{s'}/T} \rangle_{s' \in \mathcal{S}}}{\langle\langle e^{-H^{\dagger}_{ss';k}/T} \rangle\rangle_{k,s' \in \mathcal{B}_s}}, \tag{51}$$

where the infinite temperature expected loop time is

$$\tau_{\infty}^{\ell}(s) = \frac{S_N}{b_s}. \tag{52}$$

Moreover, the high-temperature expansion

$$\tau^{\ell}(s) \underset{T\to\infty}{\longrightarrow} \tau_{\infty}^{\ell}(s)\left(1 + \frac{M^{\ell}(s)}{T}\right),$$
$$M^{\ell}(s) = \langle\langle H^{\dagger}_{ss';k} \rangle\rangle_{k,s' \in \mathcal{B}_s} - \langle H_{s'} \rangle_{s' \in \mathcal{S}} \tag{53}$$

is very similar to that of the return time. The two expansions Eqs. (43) and (53) are actually identical to leading order in $1/S_N$. Thus, the condition for the presence of an optimal temperature Eq. (44) is also valid for the loop time (it is actually exact for the loop time, while it was only an approximation for the return time).

At low temperatures, the asymptotic behaviors of $\tau^{\ell}(s)$ and $\tau^{\rm r}(s)$ are also identical, except when s is the ground state. For all states including the ground states, we have at low temperatures:

$$\tau^{\ell}(s) \underset{T\to 0}{\longrightarrow} \frac{G_{(0)}}{G^{\dagger}_{s(0)}} e^{(H^{\dagger}_{s(0)} - H_{(0)})/T}. \tag{54}$$

Furthermore, there is also an optimal temperature at which the loop time can be minimum. The equation for $T_m^{\ell}(s)$ is similar to Eq. (49) and reads

$$\overline{H_{\rm eq}}\big|_{T=T_m^{\ell}(s)} = \frac{\left\langle\left\langle H^{\dagger}_{ss';k}\, e^{-H^{\dagger}_{ss';k}/T_m^{\ell}(s)} \right\rangle\right\rangle_{k,s' \in \mathcal{B}_s}}{\left\langle\left\langle e^{-H^{\dagger}_{ss';k}/T_m^{\ell}(s)} \right\rangle\right\rangle_{k,s' \in \mathcal{B}_s}}. \tag{55}$$

Globally, $\tau^{\ell}(s)$ and $\tau^{\rm r}(s)$ are expected to be similar when N is large enough, and when s is not a unique a ground state.

In Fig. 11, we focus on cases where a significant difference can be found between $\tau^{\ell}(s)$ and $\tau^{\rm r}(s)$. The cases of dimers $N = 2$ and trimers $N = 3$ are reported in Fig. 11(a). In these special cases with a single energy level (i.e., $i_{\max} = 0$) we have a simple relation independent of the state and of the temperature $\tau^{\ell}(s)/\tau^{r}(s) = 1/(1 - 1/S_N)$, which leads to $\tau^{\ell}(s)/\tau^{r}(s) = 2$ for $N = 2$ and $\tau^{\ell}(s)/\tau^{r}(s) = 6/5$ for $N = 3$.

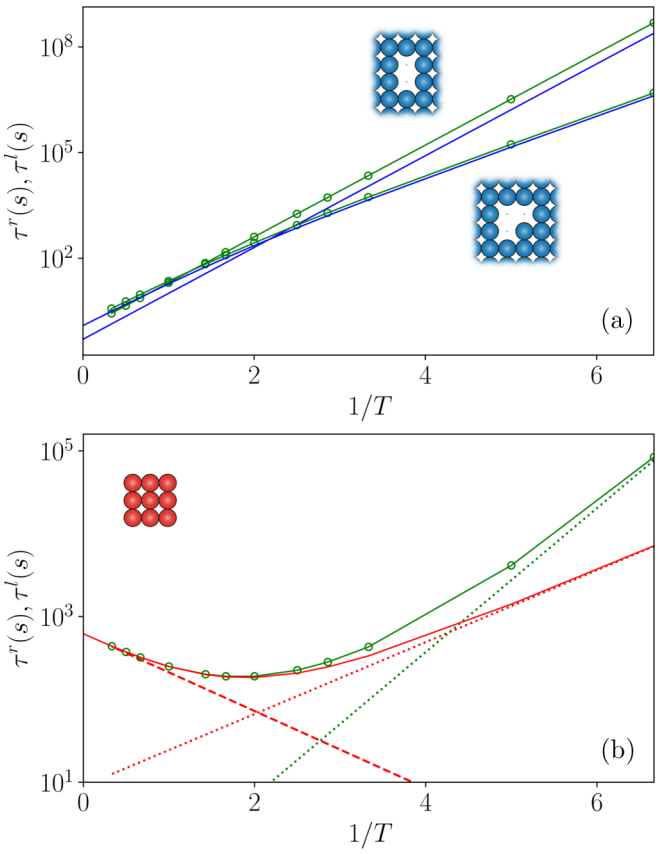

FIG. 11. Differences between expected return time $\tau^{\ell}(s)$ and loop time $\tau^{\mathrm{r}}(s)$. (a) Small vacancies with $N = 2$ and $N = 3$, vacancy DDA. (b) Square cluster with $N = 9$, cluster ED.

Another case where $\tau^{\ell}(s)$ and $\tau^{\mathrm{r}}(s)$ can be different is that of square islands at low temperature, as shown in Fig. 11(b).

VI. DISCUSSION AND CONCLUSION

To conclude, we have reported on the properties of the expected return time $\tau^{\mathrm{r}}(s)$ to a given cluster configuration s in equilibrium. We have focused on a broken-bond model that allows one to describe ED for clusters and DDA inside vacancies within a unified framework. The evaluation of $\tau^{\mathrm{r}}(s)$ from the residence time and the equilibrium probability distribution is much faster numerically than the evaluation based on the iterative evaluation method presented in Ref. [32]. In addition, the analysis of this expression leads to simple and intuitive expansions in the high and low temperature regimes, and allows one to study the optimal temperature at which $\tau^{\mathrm{r}}(s)$ is minimum. The origin of this optimal temperature can be traced back to the equilibrium optimal temperature at which the probability of observing a given low-energy state is maximum. The return time optimal temperature is found to be shifted to higher temperatures as compared to the equilibrium optimal temperature. This shift is larger for vacancies than for islands.

We hope that the investigation of the properties of cluster return times will provide useful hints for a better understanding of first passage times. Indeed, their properties are similar to those of first passage times but are much simpler to analyze. We hope that our work will motivate theoreticians and experimentalists to investigate cluster return times with various types of mass transport kinetics.

APPENDIX A: RECURSION RELATION FOR FIST PASSAGE TIMES AND ITERATIVE EVALUATION

The expected first passage time $\tau(s, \bar{s})$ from state s to state $\bar{s}$ obeys a recursion relation [32]

$$\tau(s, \bar{s}) = t(s) + \sum_{s' \in \mathcal{B}_s} p(s, s')\tau(s', \bar{s}), \tag{A1}$$

where

$$p(s, s') = t(s)\gamma(s, s'). \tag{A2}$$

In Ref. [32], we have reported on the study of first passage times from an arbitrary state s to another arbitrary state $\bar{s}$, called the target state.

The expected return time $\tau^{\mathrm{r}}(\bar{s})$ to state $\bar{s}$ can be written as a sum of the first passage times over the neighbors of $\bar{s}$ [32]:

$$\tau^{\mathrm{r}}(\bar{s}) = \sum_{s \in \mathcal{B}_{\bar{s}}} p(\bar{s}, s)\tau(s, \bar{s}). \tag{A3}$$

As discussed in Ref. [32], a numerical solution of $\tau(s, \bar{s})$ can be obtained via a simple iterative evaluation of Eq. (A1). Then, $\tau^{\mathrm{r}}(\bar{s})$ is obtained from Eq. (A3). In Fig. 12, this iterative method is shown to be in quantitative agreement with Kac's formula Eq. (9) for the cluster ED and vacancy DDA models. However, the iterative method is slower because it requires to determine $\tau(s, \bar{s})$ for all states s.

APPENDIX B: HIGH TEMPERATURE EXPANSION LINK TO THE RESULTS OF REF. [32]

1. High-temperature expansion

In Ref. [32], we have derived an expression that is convenient for the study of the high-temperature regime:

$$\tau^{\mathrm{r}}(\bar{s}) = t(\bar{s})(S_N - 1) + t(\bar{s}) \sum_{s} \tau(s, \bar{s}) \sum_{s' \in \mathcal{B}_s} (\gamma(s', s) - \gamma(s, s')). \tag{B1}$$

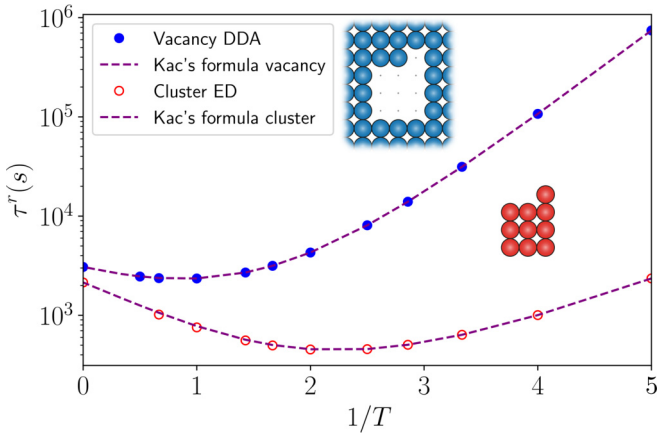

FIG. 12. Comparison of the return time $\tau^r(s)$ from Kac's formula Eq. (9) and the value obtained by iterative evaluation.

Following the same lines as in Ref. [32], we perform an expansion to linear order in $1/T$ to obtain the first correction to Eq. (37). We start with the expansion of the rates

$$\gamma(s,s') = b_{ss'} - \frac{n_{ss'}}{T}, \tag{B2}$$

where for the sake of concision, we have defined

$$b_{ss'} = b_{s's} = \sum_{k=1}^{k_{ss'}} b_{ss';k}, \tag{B3}$$

$$n_{ss'} = \sum_{k=1}^{k_{ss'}} b_{ss';k}\, n_{ss';k}. \tag{B4}$$

Inserting this expression in the expected return time Eq. (B1), we obtain to linear order in $1/T$

$$\tau^{\mathrm{r}}(\bar{s}) = \tau^{\mathrm{r}}_{\infty}(\bar{s})\left(1 + \frac{M^{\mathrm{r}}(\bar{s})}{T}\right)$$
$$M^{\mathrm{r}}(\bar{s}) = \frac{1}{b_{\bar{s}}}\sum_{s\in\mathcal{B}_{\bar{s}}} n_{\bar{s}s} + \frac{1}{S_N-1}\sum_{s}\tau_{\infty}(s,\bar{s})\sum_{s'\in\mathcal{B}_s}(n_{ss'} - n_{s's}), \tag{B5}$$

where $\tau_{\infty}(s,\bar{s})$ is the value of $\tau(s,\bar{s})$ when $T\to\infty$.

2. Expression of $M^{\mathrm{r}}(s)$ as a function of energies

Using Eq. (21), M^{r} is rewritten as

$$M^{\mathrm{r}}(\bar{s}) = -H_{\bar{s}} + \frac{1}{b_{\bar{s}}}\sum_{s\in\mathcal{B}_{\bar{s}}} H^{\dagger}_{\bar{s}s} - \frac{1}{S_N-1}\sum_{s}\sum_{s'\in\mathcal{B}_s} b_{ss'}(\tau_{\infty}(s,\bar{s})H_s - \tau_{\infty}(s,\bar{s})H_{s'}), \tag{B6}$$

where we have used Eqs. (19), and we have defined

$$H^{\dagger}_{ss'} = \sum_{k=1}^{k_{ss'}} b_{ss';k} H^{\dagger}_{ss';k}. \tag{B7}$$

We now notice that the double sum in the last line of Eq. (B6) corresponds to a sum over all possible physical moves from s to s'. We can therefore exchange s and s' in the last term of the sum, leading to

$$M^{\mathrm{r}}(\bar{s}) = -H_{\bar{s}} + \frac{1}{b_{\bar{s}}}\sum_{s\in\mathcal{B}_{\bar{s}}} H^{\dagger}_{\bar{s}s} - \frac{1}{S_N-1}\sum_{s} H_s \sum_{s'\in\mathcal{B}_s} b_{ss'}(\tau_{\infty}(s,\bar{s}) - \tau_{\infty}(s',\bar{s})). \tag{B8}$$

Now, we notice that the recursion relation Eq. (A1) can be rewritten as

$$1 = \sum_{s'\in\mathcal{B}_s}\gamma(s,s')(\tau(s,\bar{s}) - \tau(s',\bar{s})) \tag{B9}$$

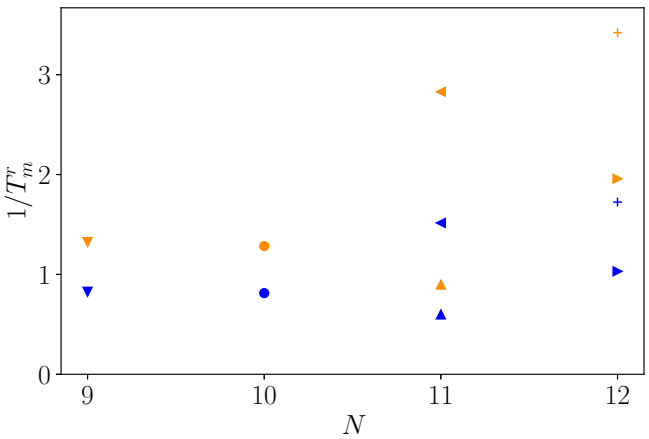

FIG. 13. Optimal return time inverse temperature $1/T^{\mathrm{r}}_m(s)$ for various states with vacancy DDA. The prediction from the high-temperature expansion Eq. (C1) is shown in orange (light) symbols.

for any $s\neq\bar{s}$. In the limit of infinite temperatures, this equation reads

$$1 = \sum_{s'\in\mathcal{B}_s} b_{ss'}(\tau_{\infty}(s,\bar{s}) - \tau_{\infty}(s',\bar{s})). \tag{B10}$$

The last term Eq. (B8) is seen to be equal to 1 from Eq. (B10) for all $s\neq\bar{s}$, so

$$M^{\mathrm{r}}(\bar{s}) = -H_{\bar{s}} + \frac{1}{b_{\bar{s}}}\sum_{s\in\mathcal{B}_{\bar{s}}} H^{\dagger}_{\bar{s}s} - \frac{1}{S_N-1}\sum_{s} H_s + \frac{1}{S_N-1}H_{\bar{s}} + \frac{1}{S_N-1}H_{\bar{s}}\sum_{s'\in\mathcal{B}_{\bar{s}}} b_{\bar{s}s'}\tau_{\infty}(s',\bar{s}). \tag{B11}$$

From Eq. (B2), the rate at infinite temperature is $\gamma_{\infty}(s,s') = b_{ss'}$, and the residence time is $t_{\infty}(s) = 1/(\sum_{\in\mathcal{B}_s} b_{ss'}) = 1/b_s$. Thus, using Eqs. (37), (A2), and (A3), we have

$$\sum_{s'\in\mathcal{B}_{\bar{s}}} b_{\bar{s}s'}\tau_{\infty}(s',\bar{s}) = b_{\bar{s}}\sum_{s'\in\mathcal{B}_{\bar{s}}} p_{\infty}(\bar{s},s')\tau_{\infty}(s',\bar{s}) = b_{\bar{s}}\tau^{\mathrm{r}}_{\infty}(\bar{s}) = S_N - 1. \tag{B12}$$

Using this relation in Eq. (B11), we find

$$M^{\mathrm{r}}(\bar{s}) = \frac{1}{b_{\bar{s}}}\sum_{s\in\mathcal{B}_{\bar{s}}} H^{\dagger}_{\bar{s}s} + \frac{1}{S_N-1}(H_{\bar{s}} - \sum_{s} H_s). \tag{B13}$$

Recombining the terms of this latter equation leads to Eq. (43).

APPENDIX C: HIGH-TEMPERATURE EXPANSION OF THE OPTIMAL TEMPERATURES

A first-order expansion of Eq. (49) in $1/T^{\mathrm{r}}_m(s)$ leads to

$$T^{\mathrm{r}}_{m,HT}(s) = \frac{\langle H^2_{s'}\rangle_{s\in\mathcal{S}\setminus s} - \langle H_{s'}\rangle^2_{s\in\mathcal{S}\setminus s} - \langle\langle H^{\dagger 2}_{ss';k}\rangle\rangle_{k,s'\in\mathcal{B}_s} + \langle\langle H^{\dagger}_{ss';k}\rangle\rangle^2_{k,s'\in\mathcal{B}_s}}{\langle H_{s'}\rangle_{s\in\mathcal{S}\setminus s} - \langle\langle H^{\dagger}_{ss';k}\rangle\rangle_{k,s'\in\mathcal{B}_s}}. \tag{C1}$$

In Fig. 13, the resulting estimate of the optimal temperature is seen to be in reasonable agreement with the observed minimum of $\tau^{\mathrm{r}}(s)$ for vacancy DDA, and to be become better as the optimal temperature increases. This agreement is expected because the optimal temperatures are rather high. For the same reason, the other estimates based on a low-temperature expansion and on the matching between low- and high-temperature expansions are inaccurate in the range of size N that we have explored.

[1] M. Giesen, Prog. Surf. Sci. **68**, 1 (2001).
[2] H.-C. Jeong and E. D. Williams, Surf. Sci. Rep. **34**, 171 (1999).
[3] R. Ganapathy, M. R. Buckley, S. J. Gerbode, and I. Cohen, Science **327**, 445 (2010).
[4] W. W. Pai, A. K. Swan, Z. Zhang, and J. F. Wendelken, Phys. Rev. Lett. **79**, 3210 (1997).
[5] C. Zaum, M. Rieger, K. Reuter, and K. Morgenstern, Phys. Rev. Lett. **107**, 046101 (2011).
[6] J.-M. Wen, J. W. Evans, M. C. Bartelt, J. W. Burnett, and P. A. Thiel, Phys. Rev. Lett. **76**, 652 (1996).
[7] M Eß er, K. Morgenstern, G. Rosenfeld, and G. Comsa, Surf. Sci. **402-404**, 341 (1998).
[8] R. E. Lake, A. Dean, N. Maheswaranathan, A. P. Lange, M. P. Ray, and C. E. Sosolik, Rev. Sci. Instrum. **79**, 013703 (2008).
[9] K. Morgenstern, E. Lægsgaard, and F. Besenbacher, Phys. Rev. Lett. **86**, 5739 (2001).
[10] K. Morgenstern, G. Rosenfeld, B. Poelsema, and G. Comsa, Phys. Rev. Lett. **74**, 2058 (1995).
[11] D. C. Schlößer, K. Morgenstern, L. K. Verheij, G. Rosenfeld, F. Besenbacher, and G. Comsa, Surf. Sci. **465**, 19 (2000).
[12] H. Watanabe and M. Ichikawa, Phys. Rev. B **55**, 9699 (1997).
[13] W. W. Pai, J. F. Wendelken, C. R. Stoldt, P. A. Thiel, J. W. Evans, and D.-J. Liu, Phys. Rev. Lett. **86**, 3088 (2001).
[14] Y. Saito, *Statistical Physics of Crystal Growth* (World Scientific, Singapore, 1996).
[15] D. C. Schlößer, L. K. Verheij, G. Rosenfeld, and G. Comsa, Phys. Rev. Lett. **82**, 3843 (1999).
[16] S. Kodambaka, S. V. Khare, V. Petrova, D. D. Johnson, I. Petrov, and J. E. Greene, Phys. Rev. B **67**, 035409 (2003).
[17] E. Hilou, D. Du, S. Kuei, and S. L. Biswal, Phys. Rev. Materials **2**, 025602 (2018).
[18] Z. Ou, L. Yao, H. An, B. Shen, and Q. Chen, Nat. Commun. **11**, 4555 (2020).
[19] S. V. Khare, N. C. Bartelt, and T. L. Einstein, Phys. Rev. Lett. **75**, 2148 (1995).
[20] O. Pierre-Louis, Phys. Rev. Lett. **87**, 106104 (2001).
[21] C. Misbah, O. Pierre-Louis, and Y. Saito, Rev. Mod. Phys. **82**, 981 (2010).
[22] A. Karim, A. N. Al-Rawi, A. Kara, T. S. Rahman, O. Trushin, and T. Ala-Nissila, Phys. Rev. B **73**, 165411 (2006).
[23] K. C. Lai, D.-J. Liu, and J. W. Evans, Phys. Rev. B **96**, 235406 (2017).
[24] A. Bogicevic, S. Liu, J. Jacobsen, B. Lundqvist, and H. Metiu, Phys. Rev. B **57**, R9459 (1998).
[25] G. Mills, T. R. Mattsson, L. Mllnitz, and H. Metiu, J. Chem. Phys. **111**, 8639 (1999),.
[26] N. Combe and H. Larralde, Phys. Rev. B **62**, 16074 (2000).
[27] O. U. Uche, D. Perez, A. F. Voter, and J. C. Hamilton, Phys. Rev. Lett. **103**, 046101 (2009).
[28] B. C. Hubartt and J. G. Amar, J. Chem. Phys. **142**, 024709 (2015).
[29] M. Shen, J.-M. Wen, C. J. Jenks, P. A. Thiel, D.-J. Liu, and J. W. Evans, Phys. Rev. B **75**, 245409 (2007).
[30] M. Basham, P. Mulheran, and F. Montalenti, Surf. Sci. **565**, 289 (2004).
[31] K. Morgenstern, E. Lægsgaard, and F. Besenbacher, Phys. Rev. B **66**, 115408 (2002).
[32] F. Boccardo and O. Pierre-Louis Phys. Rev. Lett. **128**, 256102 (2022).
[33] M. Kac, Bull. Am. Math. Soc. **53**, 1002 (1947).
[34] D. Aldous and J. A. Fill, Reversible Markov chains and random walks on graphs (2002), http://www.stat.berkeley.edu/~aldous/RWG/book.html.
[35] Here and in the following, *expected* refers to an expected value and is a synonym of *average*.
[36] A. J. Guttmann, *Polygons, Polyominoes and Polycubes*, Lecture Notes in Physics, Vol. 775 (Springer, Dordrecht, 2009).
[37] G. H. Gilmer and P. Bennema, J. Appl. Phys. **43**, 1347 (1972).
[38] G. Gilmer and P. Bennema, J. Cryst. Growth **13-14**, 148 (1972), Third International Conference on Crystal Growth.
[39] M. Kotrla, Comput. Phys. Commun. **97**, 82 (1996), High-Performance Computing in Science.
[40] J. R. Sanchez and J. W. Evans, Phys. Rev. B **59**, 3224 (1999).
[41] O. Pierre-Louis and T. L. Einstein, Phys. Rev. B **62**, 13697 (2000).
[42] Such a model can, for example, be obtained in the limit of lattice models with a small attachment rate, which correspond to the limit of small Q in Refs. [49,50].
[43] R. Livi and P. Politi, *Non-equilibrium Statistical Physics* (Cambridge University Press, Cambridge, 2017).
[44] I. Jensen and A. J. Guttmann, J. Phys. A: Math. Theor. **33**, L257 (2000).
[45] Since the number of possible positions of an isolated particle in a vacancy is at most equal to N, S_N for vacancies is at most N times smaller than S_N for clusters. Hence, the elimination of these configurations can only lead to algebraic (power-law) corrections. As a consequence, the exponential growth rate λ is the same for clusters and vacancies.
[46] L. Lovász, Combinatorics, Paul Erdős is Eighty **2**, 4 (1993).
[47] Since each move has a direction from state s to state s', our graph is a directed graph and d_s is the out degree of s. For simplicity, we call d_s the degree of s.
[48] Since there is always a pair of indices s', k such that $\ell^{\dagger}_{s;q} = \ell^{\dagger}_{ss';k}$, we see that (40) is simply a different way to sum over the moves as compared to (39). Indeed, in the transitions from s to $s' \neq s$, we have to sum over all reattachment moves except those that take the system back to s, and we have

$$b_s = \sum_{s' \in \mathcal{B}_s} \sum_{k=1}^{k_{ss'}} b_{ss';k} = \sum_{\mathrm{q}=1}^{\ell_s} \frac{\ell^{\dagger}_{s;q} - 1}{\ell^{\dagger}_{s;q}}$$

which leads to (40).
[49] L. Gagliardi and O. Pierre-Louis, J. Comput. Phys. **452**, 110936 (2022).
[50] B. Marguet, F. D. A. Aarão Reis, and O. Pierre-Louis, Phys. Rev. E **106**, 014802 (2022).